



Time and space-resolved laser-induced breakdown spectroscopy on molybdenum in air

Eshita Mal¹ · Rajendhar Junjuri² · Manoj Kumar Gundawar² · Alika Khare¹

Received: 5 August 2020 / Accepted: 18 February 2021 / Published online: 17 March 2021
© The Author(s), under exclusive licence to Springer-Verlag GmbH, DE part of Springer Nature 2021

Abstract

In the present work, laser-induced plasma (LIP) of Mo is studied using both time and space resolved laser-induced breakdown spectroscopy (LIBS) in air as a function of incident laser energy. For this a second harmonic Q-switched Nd:YAG laser having pulse width of 7 ns and repetition rate of 1 Hz is used. The Boltzmann plot method is employed to estimate the plasma temperature of LIP using MoI and MoII lines separately. The stark-broadened profile of MoI-313.2 nm is exploited to measure the electron density. The temporal study in the time delay range of 0.5–5.0 μs shows that both the parameters, decay with the increase in delay time but increases with the increase in laser energy. It is observed that the plasma temperature estimated for MoII lines is higher than that of the MoI lines during the initial stage of plasma formation, delay time of 0.5–1.0 μs , but at a later time scale, both these species are found to possess nearly the same values of the temperature, indicating the coexistence of thermal equilibrium among the Mo atoms and ions in LIP. Therefore, in the second part of the experiment, time-integrated spatial evolution of the LIP of Mo is studied at a fixed delay of 2 μs as a function of axial distance normal to the target. It is found that emission intensity (MoI and MoII both), plasma temperature, and electron density initially increase with the increase in distance from the target, attains maximum value and then falls down. The Mc-Whirter criteria is applied to test the validity of local thermodynamic equilibrium (LTE). The relaxation time and diffusion length are estimated in time and space resolved studies respectively to take care of the transient and inhomogeneous nature of the LIP. The optical thin condition of LIP is verified by employing the branching ratio method. From these studies, a suitable spatio-temporal is identified where the LTE and optically thin plasma condition hold along with a high signal to noise ratio.

1 Introduction

In the last few years, there is increasing attention for laser-induced breakdown spectroscopy (LIBS) as a spectrochemical analytical tool [1]. LIBS has some inherent properties that make it superior to other analytical techniques [2, 3]. It is free from any sample preparation, applicable to any sample irrespective of its physical state (solid, liquid, gases), non-destructive or minimally destructive technique as a sub-microgram sample is enough for analysis by single laser shot ablation, capable of multi-elemental analysis simultaneously, simple, versatile and only optical access to the target and plasma radiation are required. The LIBS has potential

for both in-situ and ex-situ analysis in the hostile and hazardous environment [4–6]. Due to all these salient features, LIBS is being realized as a handy tool in every field of science [1, 7–9]. In the LIBS technique, a high-power pulsed laser is focused on to the target under investigation to furnish a high density, high-temperature luminous laser-induced plasma (LIP). Immediately after the commencement of LIP, it starts expanding in the surrounding medium, cools down, and emits the characteristic line spectrum of the constituent elements making it feasible for the identification of the constituent elements [10]. In spite of the various applications of LIBS, the understanding of the dynamics of LIP remains insufficient and none of the available theoretical models are capable of unfolding the complex phenomenon in the laser-matter and laser-plasma interaction [11–13]. The dynamics of LIP is strongly affected by the experimental parameters which in turn control the evolution of the electron density and plasma temperature. These plasma parameters influence the analytical performance of the LIBS technique and are very much dependent on the selection of the experimental

✉ Eshita Mal
m.eshita@iitg.ac.in

¹ Indian Institute of Technology Guwahati, Guwahati, India

² Advanced Centre of Research in High Energy Materials, University of Hyderabad, Hyderabad, India

conditions which include laser parameters (i.e. laser energy, pulse duration and wavelength), chemical, physical and mechanical properties of the target material, the geometry of laser focusing to generate the LIP, collection optics for the detection of LIP radiation, the nature and pressure of the ambient gas and temporal as well as spatial evolution of transient inhomogeneous LIP [14–16]. The investigation on LIP as a function of various experimental parameters are well documented but limited to either only time-resolved or only space resolved one [17–23]. There is a scarcity of the number of publications addressing both the temporal and spatial evolution of the LIP under a similar experimental situation [11]. In the present manuscript, the spatio-temporal evolution of LIP of Mo in air is represented. The molybdenum is a promising candidate in nuclear fusion reactor as it possesses a high melting point, low sputtering yield, and high reflectivity for a broad range of wavelengths [24–26] and thus it is suitable for the first mirror in International Thermonuclear Experimental Reactor (ITER). Inside a fusion reactor in the harsh environment, the bombarding of high-energy particles, exposure to highly intense electromagnetic radiation, and deposition degrade the mirror and thus reduces its lifetime. To maintain and improve the quality of the first mirror, there is a need to perform online cleaning and monitoring. For this purpose, due to the inherent salient features of LIBS technique, it is suitable for the analysis of plasma-facing component. Besides the application of Mo in a fusion reactor, it has many other applications, such as the nanostructures of compound elements of Mo like MoO_3 , MoS_2 etc., are beneficial in sensing and optoelectronic devices [27], deposition of high quantity thin films via pulsed laser deposition (PLD), micro structuring through laser ablation etc. in it. There are very few studies on LIP of Mo via the LIBS technique. Moreover, there is also a scarcity of atomic database for Mo transitions which is essential for LIP characterization using LIBS. The time and space-resolved LIBS for various incident laser energies on Mo target is reported in the present manuscript. The suitable temporal as well as spatial window are identified for the validity of LTE and optical thin condition of the LIP.

2 Experimental details

The experimental setup to record the temporal evolution of LIP is reported in our earlier work [28]. Briefly, a Q-switched Nd: YAG laser (INNOLAS Split light 1200) working at second harmonic ($\lambda = 532$ nm), pulse duration of 7 ns and repetition rate of 1 Hz capable of delivering a maximum of 600 mJ energy is focused on the Mo target (99.9% purity) by a Plano convex lens1 of focal length 15 cm to a focal spot of 230 μm . The target is placed on to an X–Y linear translation stage to move the target sample across the

laser beam to provide a fresh surface for each laser shots and avoid the formation of a deep crater.

For recording the temporal evolution of LIP, the radiation from the emitted LIP is collected at an angle of 45° with respect to laser pulse by a system of collection optics, the combination of mirrors and lens and focused on to the optical fiber having core diameter of 600 μm . The other end of which is coupled to the entrance of an echelle spectrograph (Andor Mechelle ME5000) equipped with ICCD detector interfaced to the computer enabling the recording of the spectrum over a wide wavelength range of 200–850 nm in one single-shot acquisition. The ICCD is operated in a gated mode to record the temporal evolution of the emission spectra as a function of delay time with respect to the laser pulse. For the case of time-resolved studies, the spectra from LIP of Mo is recorded in the time range of 0.5–5.0 μs in a step of 0.5 μs by maintaining the gate width of 0.5 μs throughout the experiment.

The experimental setup used for space-resolved spectroscopic analysis of the LIP is nearly similar to that of the temporal evolution with slight difference in collection geometry of the LIP emission. The setup is sketched in Fig. 1. In space-resolved studies, the ICCD gate delay is kept fixed at 2 μs with respect to laser pulse.

In this, lens2 of focal length of 10 cm is used in one to one the configuration to form an inverted image of the plasma with a magnification of unity. The laser beam is assumed to be along z-axis, the plasma emission is collected using an optical fiber of 400 μm core diameter positioned in the image plane (x – z plane) as shown in Fig. 1. The fiber is positioned on a motorized linear-translational stage. The plasma is imaged with the magnification of unity (one-to-one correspondence) on the optical fiber of diameter 400 μm . Therefore, the spectra are recorded within the small window having cross-sectional area of the fiber integrated along y axis. Thus, the movement of fiber along the plasma expansion direction enables the record of the space resolved spectra of LIP. The scanning step is maintained at 0.4 mm to match the diameter of the optical. These space-resolved signals are transmitted through the optical fiber, fed to the echelle spectrometer.

3 Results and discussion

LIP is characterized via the intensity of lines in its emitted spectrum and by analyzing the spectra emission, the plasma temperature and electron density are estimated. The estimation of the plasma parameters are based on the assumption of local thermodynamic equilibrium (LTE) and optical thin radiation condition. In the following sub-sections, results obtained from time-resolved LIBS studies at different delay time with respect to incident of laser pulse and space

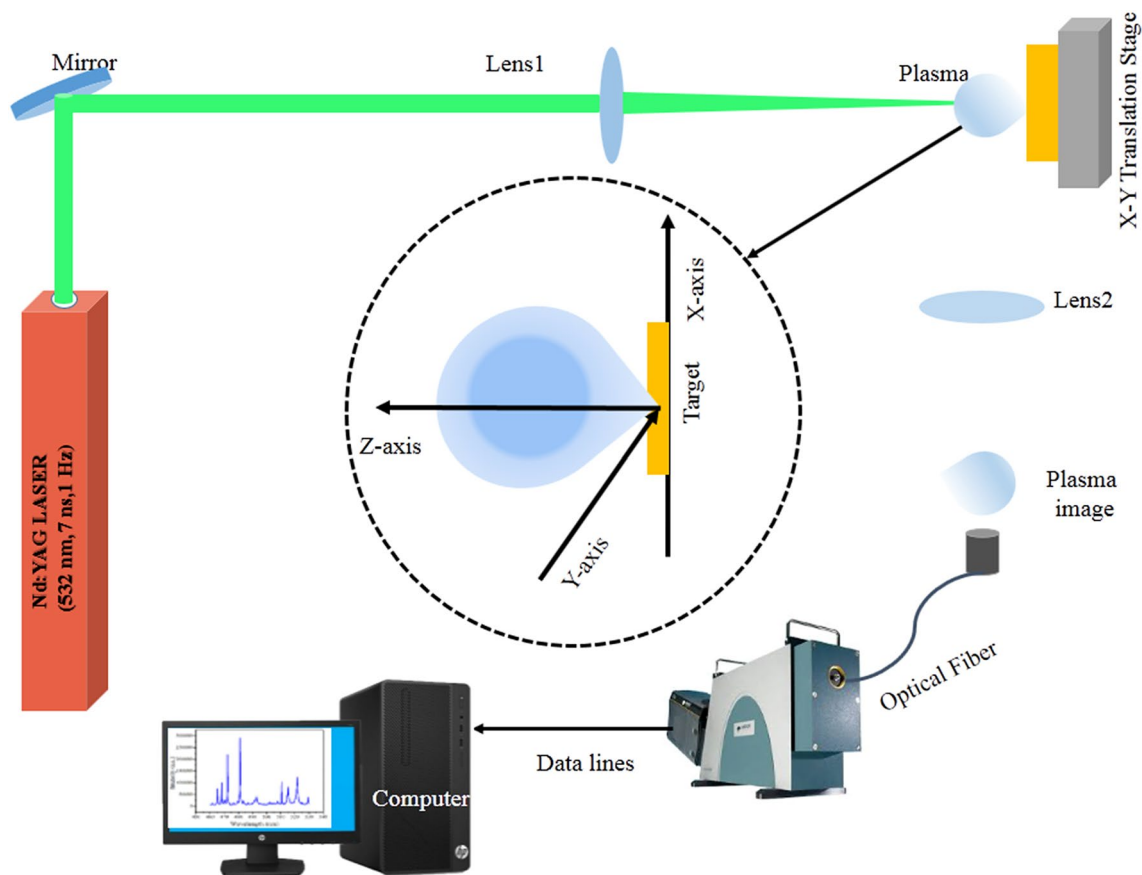


Fig. 1 Schematic of experimental setup for recording spatially resolved spectra from LIP of Mo in air

resolved LIBS studies along the axial direction of plasma expansion presented.

3.1 Time-resolved studies of LIP of Mo

The temporal evolution of LIP is recorded in the range of 0.5–5 μ s delay with respect to the laser pulse. The time evolution of MoI as well as MoII line intensity and measurement of plasma temperature and electron density in the LIP of Mo are discussed below.

3.1.1 Temporal evolution of emission spectra of LIP of Mo

The temporal evolution of LIP spectra of Mo recorded at four laser energies of 25, 50, 75 and 100 mJ in the spectral range of 220–850 nm. The expanded view of the spectra in the range of 277–288 and 550–560 nm are shown in Fig. 2a and b, respectively for the incident laser energy of 25 mJ. From the spectra, several MoI and MoII lines are identified using NIST database [29] and Kurucz database [30].

The spectral range of 287–288 nm is mainly comprised of ionic lines of Mo while that of the 550–570 nm is attributed to atomic lines. The temporal variation of

MoII-248.4.8 nm and MoI-550.6 nm lines at four laser energies are fitted to an exponential decay function to estimate the decay time. The variation of decay time with respect to the incident laser energies for MoII-284.8 and MoI-557.0 nm are shown in Fig. 3a. It is observed that the decay of ionic lines is faster than that of the atomic lines. The decay time of MoII-284.8 nm line is 0.75 (± 0.01), 1.15 (± 0.04), 1.16 (± 0.03) and 1.18 (± 0.04) μ s and that of the MoI-550.6 nm lines is 1.02 (± 0.04), 1.24 (± 0.4), 1.26 (± 0.03) and 1.27 (± 0.01) μ s for the incident laser energies of 25, 50, 75 and 100 mJ, respectively.

Due to the higher kinetic energy, ionic lines decay faster than that of the atoms. In both cases, decay time increases with the increase in the incident laser energy to a certain extent but beyond 75 mJ there is hardly any change. The temporal variation of signal to noise ratio (SNR) [31, 32] MoI-557.0 nm (as an example) at various incident laser energy is shown in Fig. 3b. It is observed that the SNR increases up to 3.5 μ s for each incident laser energy and beyond this, it falls down with delay time. This gives an indication that the detection of spectra with high SNR in the LIP emission spectrum should be recorded in this optimized temporal window. A similar range of optimized

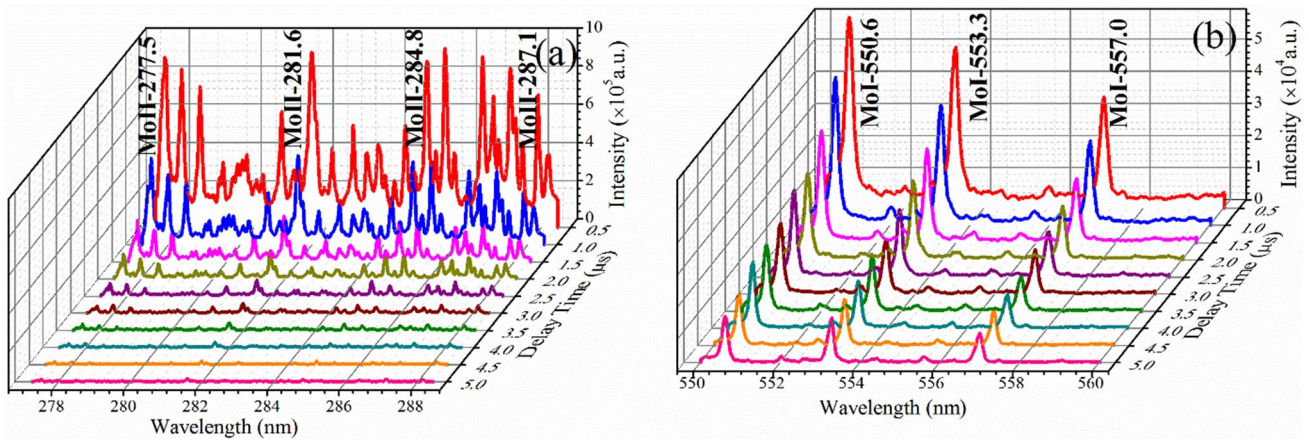


Fig. 2 Expanded view of the temporal variation of **a** Ionic lines in the spectral range 277–288 nm, **b** atomic lines in the spectral range 550–560 nm

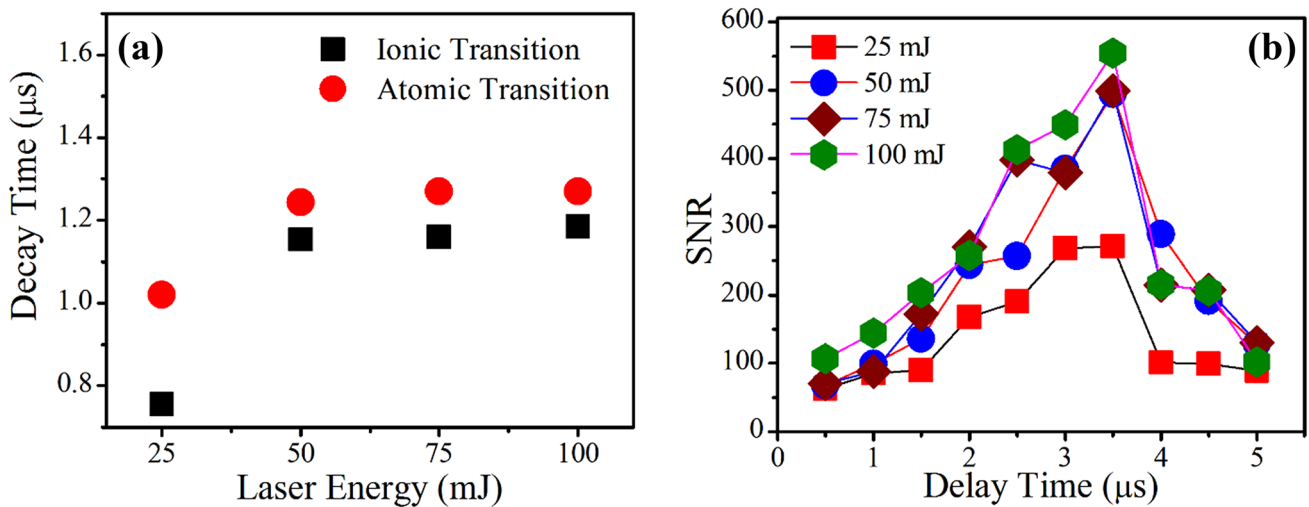


Fig. 3 Variation of the decay time of **a** MoII-284.8 nm and MoI-550.6 nm transition and **b** SNR as a function of incident laser energy

window is observed for all the spectral line in the present case.

3.1.2 Temporal evolution of plasma temperature and electron density of LIP of Mo

Assuming that the LTE prevails in the LIP and emits optically thin lines, the population distribution of energy levels is governed by the Boltzmann distribution law. The line intensity of transition I_{nm} from an upper level of n to a lower level m is related to its upper energy state E_n , and is given by the following relation [33, 34]

$$\ln \left(\frac{I_{nm} \lambda_{nm}}{g_n A_{nm}} \right) = -\frac{1}{k_B T_e} E_n + \ln \left(\frac{F N_s}{U_s(T_e)} \right), \quad (1)$$

where λ_{nm} is the wavelength of corresponding radiation, g_n is the statistical weight of the upper level, A_{nm} is the transition probability, k_B is the Boltzmann constant, T_e is the plasma temperature, h is the Planck constant, c is the velocity of light, N_s and $U_s(T_e)$ are the number density and partition function of the particular species ‘s’(atoms/ions) of an element under consideration and F is an experimental factor. The plot of left-hand side of the Eq. (1) against E_n , the upper-level energy, for several transitions is a straight line. The temperature of the species can be thus obtained from the slope of the equation i.e. $1/k_B T_e$ without requiring the information about partition function. Accuracy of the temperature measurement from the Boltzmann equation may be improved by involving a large number of different lines having upper energy states widely apart [35]. The Boltzmann plot, Eq. (1) is used to estimate the plasma temperature

Table 1 Spectroscopic data of MoI lines used for plasma temperature estimation

λ (nm)	A_{nm} (10^7s^{-1})	Lower level energy E_m (eV)	Upper level energy E_n (eV)	g_m	g_n
357.0	7.2	3.178	6.650	15	15
406.9	3.25	2.080	5.126	13	11
423.2	3.17	2.076	5.004	9	11
438.1	2.93	2.080	4.909	13	13
453.6	5.00	3.501	6.233	13	15
476.0	4.67	2.646	5.250	11	13
550.6	3.61	1.335	3.586	5	7
553.3	3.72	1.335	3.575	5	5
557.0	3.30	1.335	3.560	5	3
592.8	5.30	3.586	5.676	7	9

Table 2 Spectroscopic data of MoII lines used for plasma temperature estimation

λ (nm)	A_{nm} (10^7s^{-1})	Lower level energy E_m (eV)	Upper level energy E_n (eV)	g_m	g_n
230.4	1.609	3.425	8.804	12	10
269.2	1.382	3.437	8.040	10	8
283.1	1.132	4.166	8.543	12	13
363.5	0.5531	3.141	6.551	8	10
374.2	1.90	4.499	7.811	6	4

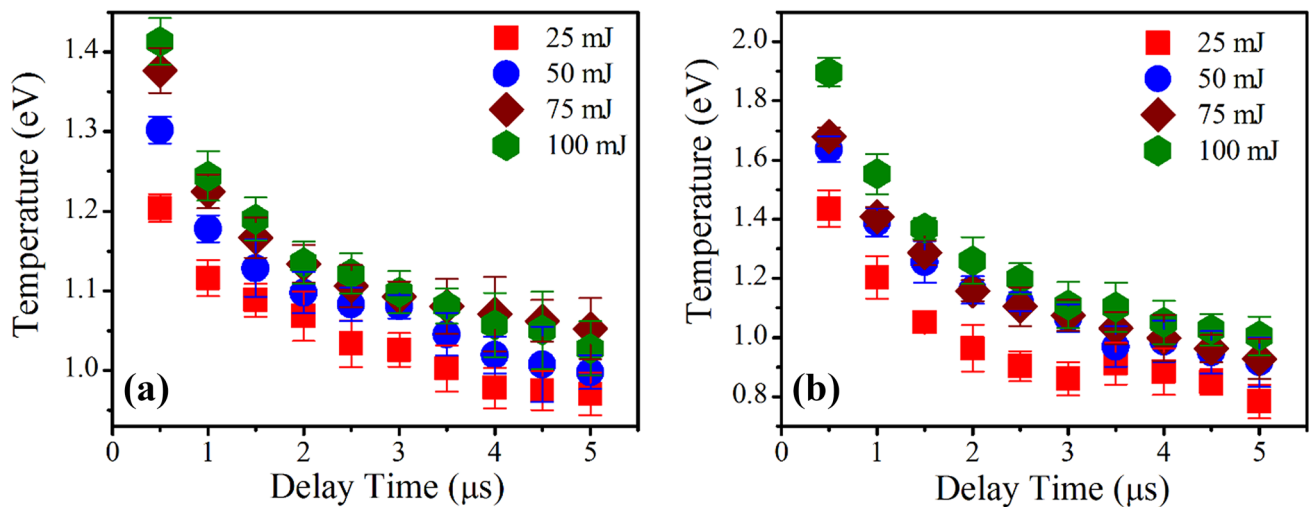
using a large number of MoI and MoII transitions having a wider spread over upper level energies. The atomic spectroscopic data required in Eq. (1) for MoI and MoII are listed in Tables 1 and 2 respectively.

The temporal variation of plasma temperature as a function of incident laser energy from MoI and Mo II lines are shown in Fig. 4a and b, respectively. It is observed from the temporal evolution of the plasma temperature, it is decreasing as the delay time increases, in both the cases, MoI and MoII lines but increases with the increase in incident laser energy. In the initial delay range of 0.5–1.0 μs the range of temperature is higher for the MoII lines than that of the MoI but at a later time range of 1.5–5 μs the temperature in both the case possess similar values. The difference in the temperature is due to the non-coexistence of equilibrium of atomic and ionic species among themselves at the initial stage of the formation of plasma [36] whereas at later stage there is the coexistence of thermodynamic equilibrium between neutral atoms and ions.

Electron density is an important plasma parameter that is used to describe the plasma environment and is also crucial for establishing thermodynamic equilibrium. One of the most powerful spectroscopic techniques to determine the electron number density with reasonable accuracy is the measurements of the Stark-broadened line profile of an isolated atom or singly charged ion. The full width half maximum (FWHM) of the Stark-broadened line, $\Delta\lambda_{1/2}$, is related to the electron density by the expression [34].

$$\Delta\lambda_{1/2} = 2w\left(\frac{N_e}{10^{16}}\right) + 3.5A\left(\frac{N_e}{10^{16}}\right)^{1/4} \left[1 - 1.2N_D^{-1/3}\right]w\left(\frac{N_e}{10^{16}}\right), \quad (2)$$

w is the electron impact width parameter, A is the ion broadening parameter and N_D is the number of particles in the Debye sphere. The first term on the right side of Eq. (2) represents the broadening due to electron contribution and the second term is the ion correction factor. The electric field that causes Stark effect in LIP results primarily from

**Fig. 4** Temporal variation of plasma temperature from **a** atomic and **b** ionic lines as a function of incident laser energy

collisions with electrons, with small contributions due to collisions with ions. Therefore, the second term can be neglected and the expression for $\Delta\lambda_{1/2}$ can be simplified to Eq. (3).

$$\Delta\lambda_{1/2} = 2w \left(\frac{N_e}{10^{16}} \right). \quad (3)$$

The electron density in LIP of Mo is estimated using the stark-broadened profile of MoI-313.2 nm line using Eq. (3). For this, the electron impact width parameter is taken from the literature [37]. The line profile of MoI-313.2 nm, fitted to Lorentzian function at a delay time of 0.5 μ s is shown in Fig. 5a. The temporal variation of electron density as a function of incident laser energies from Eq. (3) are shown in Fig. 5b. It decreases with the delay time. The variation in the electron density with the incident laser energy is more prominent in the initial temporal window of 0.5–1.5 μ s as compared to that of the later delay time.

From the Figs. 2, 4 and 5b it is evident that the plasma emission intensity of MoI and MoII lines, plasma temperatures, and electron density decrease with the increase in delay time but increase with the increase of the incident laser energy. The decrease in plasma emission intensity, electron density, and plasma temperature with the delay time after the termination of the laser pulse is due to the three mechanisms i.e. thermal conduction, expansion, and radiative cooling [38]. This is due to the fact that with the incident of laser on to the target, plasma is generated by the initial part of laser pulse while its trailing part heats the plasma. During the laser pulse, plasma expands isothermally but after the end of the laser pulse there is no external source of energy available for the plasma. So, LIP expands adiabatically in the surrounding air and loses its energy which results in

the decrease in plasma emission intensity as well plasma temperature and electron density. The increase in incident laser energy results in higher mass ablation and the plasma emission intensity and plasma parameters increases for the incident laser energy of 25–75 mJ but at the higher energy of 100 mJ the increment is not significant which may be due to the plasma shielding [17, 39].

3.1.3 Assessment of local thermodynamic equilibrium (LTE) in LIP of Mo

The accuracy of estimation of plasma temperature depends on the validity of the LTE in LIP. Due to the highly transient and inhomogeneous nature of the LIP, the assessment of LTE is performed in three different cases i.e. (1) stationary and homogeneous, (2) transient but homogeneous and (3) stationary but inhomogeneous [40].

In the first case, the LIP can be described to be in LTE if the collisional process is dominant over the radiation process. For this condition, the electron density needs to satisfy the following inequality known as Mc-Whirter criteria [41]

$$N_e (\text{cm}^{-3}) \geq 1.6 \times 10^{12} T_e^{1/2} (\Delta E_{nm})^3, \quad (4)$$

where T_e and ΔE_{nm} are expressed in kelvin and eV respectively. To assure that the LIP is in LTE, the condition expressed in Eq. (4) should hold for the largest value of ΔE_{nm} . Since ΔE_{nm} decreases with increasing values of the level quantum number, the ground level, and the first excited level, corresponding to the first resonance transition, are usually considered for the evaluation of LTE in LIP.

In the second case, the temporal evolution of the parameters should be sufficiently slow so as to have sufficient time

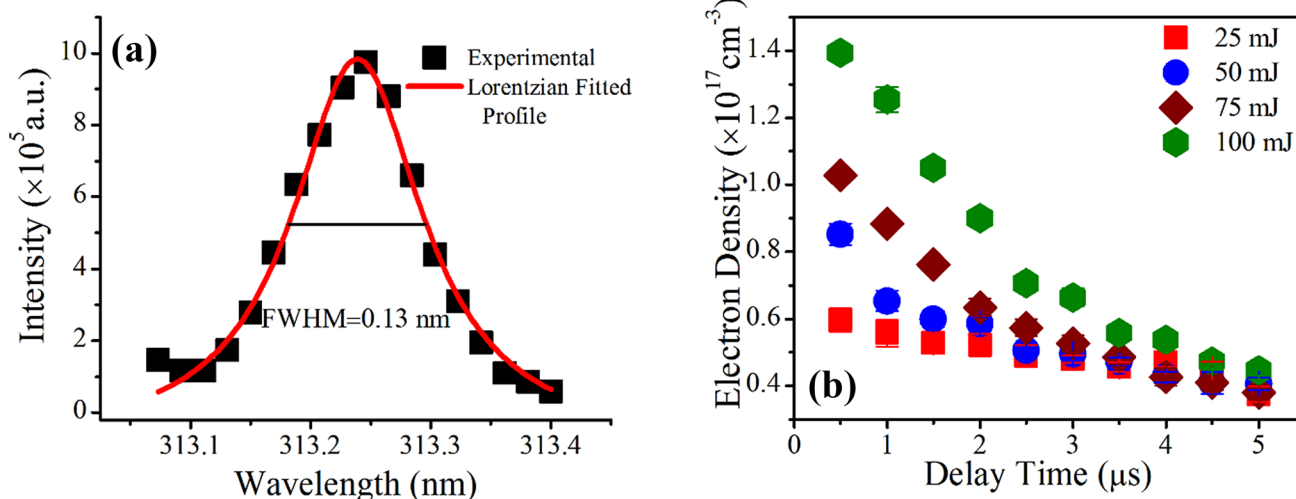


Fig. 5 a Lorentzian fitted profile of MoI-313.2 nm at 0.5 μ s delay and b variation of electron density as function of incident laser energy

to attain the thermodynamic equilibrium. This is given by the following inequalities [40]

$$\frac{T_e(t + t_{rel}) - T_e(t)}{T_e(t)} \ll 1, \tag{5}$$

$$\frac{N_e(t + t_{rel}) - N_e(t)}{N_e(t)} \ll 1, \tag{6}$$

where t_{rel} is the relaxation time, the time required for the establishment of excitation and ionization equilibrium, given by [40]

$$t_{rel} = \frac{6.3 \times 10^{-4}}{N_e f_{nm}(g)} \Delta E_{nm} (kT_e)^{\frac{1}{2}} \exp\left(\frac{\Delta E_{nm}}{kT_e}\right). \tag{7}$$

The third situation, stationary and inhomogeneous plasma, the diffusion length of the species in LIP should be shorter than the variation length of electron number density and temperature. These can be described at location x in LIP [40]

$$\frac{T_e(x + \lambda_{diff}) - T_e(x)}{T_e(x)} \ll 1, \tag{8}$$

$$\frac{N_e(x + \lambda_{diff}) - N_e(x)}{N_e(x)} \ll 1, \tag{9}$$

λ_{diff} is the diffusion length given by following equation [40],

$$\lambda_{diff} = 1.4 \times 10^{12} \frac{(kT)^{3/4}}{N_e} \left(\frac{\Delta E_{nm}}{M_A f_{nm}}\right)^{1/2} \exp\left(\frac{\Delta E_{nm}}{2kT_e}\right), \tag{10}$$

where M_A is the atomic mass of the element emitting the transition and f_{nm} is the corresponding oscillator strength.

In case of the temporal evolution of the LIP, LTE is tested in first two situations. The temporal variation of the minimum required value of electron density from Eq. (4) as function of incident laser energy is shown in Fig. 6a. On comparing it with Fig. 5b, it is found that the electron density in the present experimental condition is nearly two orders of magnitude larger than minimum electron density as per McWhirter criteria thus validating the LTE. In the next case, the variation of relaxation time estimated using Eq. (7) as a function of delay time at various laser energy is shown in Fig. 6b. The calculated relaxation time is of the order 10^{-10} s and is significantly shorter than the typical decay time of LIP which is of the order of 10^{-6} s in the present case, Fig. 3a, thus confirming the validity of LTE under the transient nature of LIP.

3.1.4 Temporal evolution of optical thin condition of LIP of Mo

The measurement of temperature in LIP via using the Boltzmann plot method and the determination of electron density by Stark broadening effect not only require the validity of LTE condition but also the LIP should be optically thin for the emitted lines being employed for this purpose. If the LIP is not optically thin, then the spectral lines under consideration for the characterization suffer from self-absorptions [42]. Due to this, the spectral line profile will exhibit distortion in the line profile leading to enormously large error in the determination of electron density and plasma temperature. Undistorted spectral line profile and good linear fitting of Boltzmann plot ensure the optical thin condition of LIP. Under the optically thin condition, the intensity of the lines should be in accordance with the following equation [33, 43]:

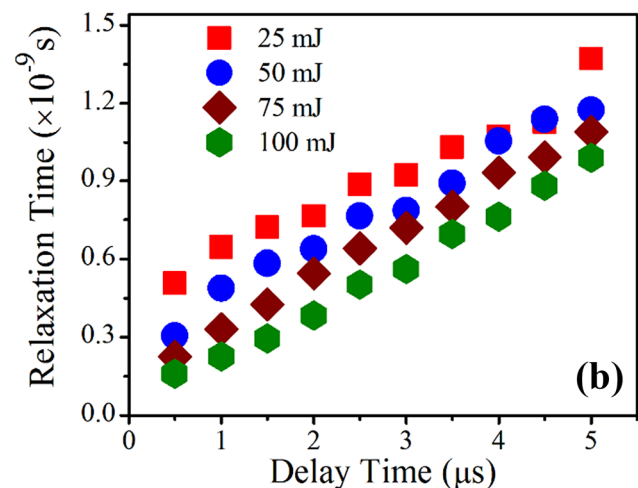
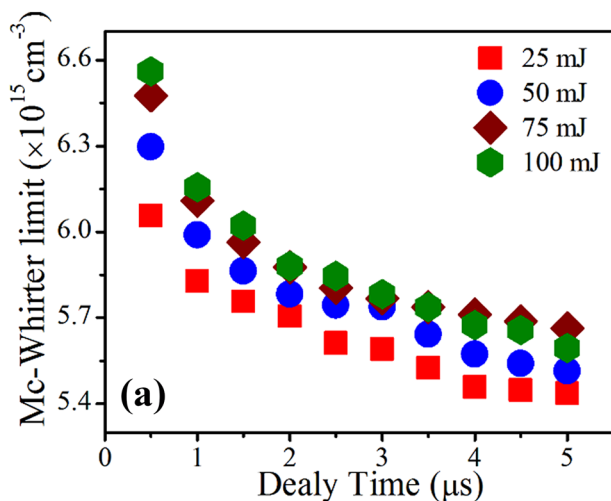


Fig. 6 Temporal evolution of a minimum electron density for LTE and b relaxation time at different laser energies

$$\frac{I_1}{I_2} = \frac{g_1 A_1 \lambda_2}{g_2 A_2 \lambda_1} \quad (11)$$

The value of the experimental intensity ratio in accordance with Eq. (11) confirms the LIP to be optically thin.

The theoretical value of intensity ratios of MoI-568.9/ MoI-579.1 is 1.16. The spatial variation of the experimental branching ratio is shown in Fig. 7 and the corresponding theoretical value from Eq. (11) is also marked with the solid line. The variation in the experimental intensity ratios 1.41–1.23, 1.58–1.26, 1.62–1.17 and 1.61–1.29 for the incident laser energies of 25, 50, 75 and 100 mJ respectively. The close proximity of the value of branching ratio obtained experimentally with that of the theoretical value is observed in the range of 1.5–4.5 μs confirming the optical thin condition in the LIP of Mo for this particular temporal window as seen from Fig. 7.

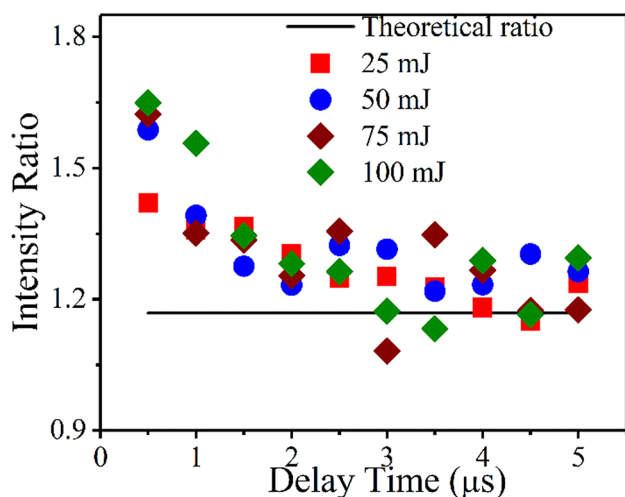


Fig. 7 Temporal variation of the intensity ratio of MoI568.9/ MoI579.1

3.2 Space-resolved studies of LIP of Mo

The LIP expansion is inhomogeneous in the perpendicular direction target surface. In the following sections results obtained from the space-resolved studies are described.

3.2.1 Axial profile of emission spectra

The LIP emission spectra are recorded at a different locations along the axial expansion direction (z axis) of the LIP of Mo using the experimental set up shown in Fig. 1. The intensity profile along the axial direction of the plasma plume for the MoII-284.8 nm and MoI-550.6 nm lines at various laser energies are shown in Fig. 8a and b, respectively. From the axial distribution of plasma emission intensity, it is observed that the maximum in the emission intensity for ionic lines appears nearer to the target surface than that of the atomic lines. The ionic transition reaches a maximum at a distance of 1.6 mm distance from the target surface for the laser energy of 25 mJ and for other higher laser energies at 2.0 mm. The atomic transition attains maximum intensity at 2.4 mm distance from the target for the incident laser energy of 25–75 mJ but for 100 mJ this distance is extended 3.2 mm similar trend has been reported in the literature [11, 44]. The velocities of ions and atoms are different in the LIP and possess the different persistent time as seen from temporal studies Sect. 3.1.1. The persistence time of ions are less than that of the atoms as seen from the temporal study. As well as the kinetic energy of the ions are higher than the atoms, so the maxima in the ionic intensity appears close to the target surface as that of the atomic transition. The intensity of MoII-284.8 nm lines increases as the incident laser energy increase and after attaining the maxima in the ionic intensity there is a sharp decrease. While for MoI-557.0 nm line, the variation in intensity as a function of laser energy is not prominent as compared to ionic line, but its intensity extends to a higher axial distance for higher energy. This is due to the fact that with higher incident laser energy, the plasma

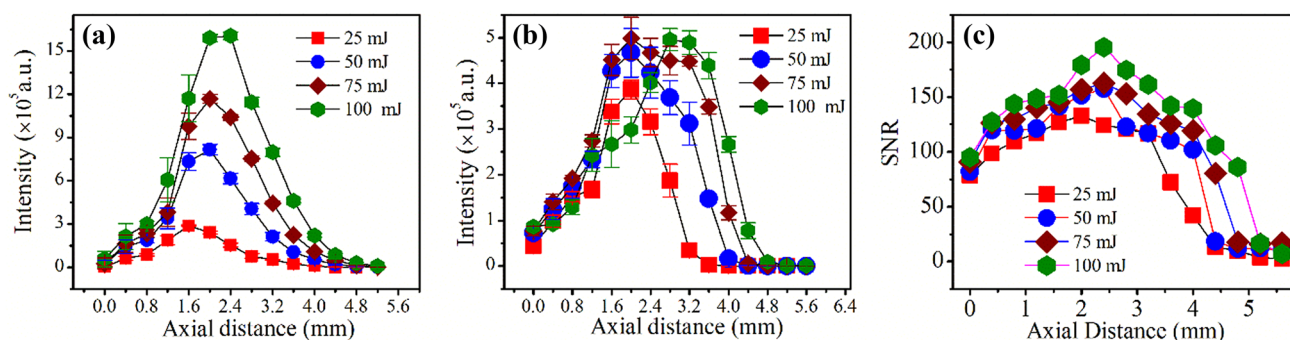


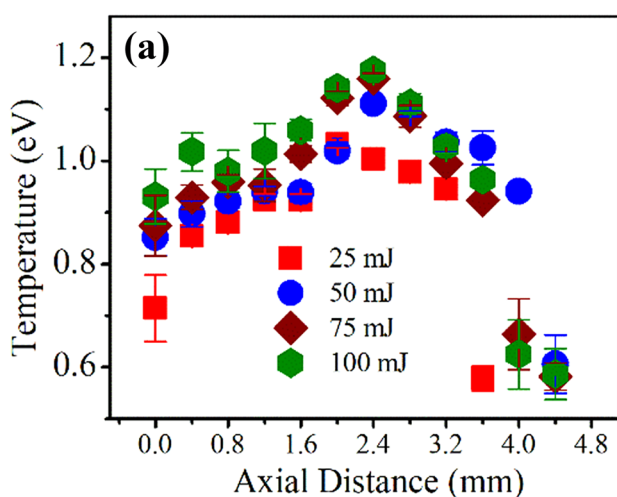
Fig. 8 Intensity variation of **a** MoII-284.8 nm, **b** MoI-550.6 nm along the axial expansion direction of the plasma and **c** SNR as a function laser energy

plume length increases, and the emission from higher stages of ionization results from the hot inner core of the LIP while emission from neutral or lower stages of ionization occur in the outer part of the LIP, so the atomic transition reaches maximum towards the extended location as compared to that of ionic transition. It is concluded that intensity for both the MoI and MoII transitions increases up to a certain distance and after attaining the maximum intensity these start to decrease due to the various energy loss mechanisms [14, 45, 46]. The spatial variation of SNR as a function of energy as obtained from MoI-557.0 nm line is shown in Fig. 8c. It is seen that SNR increases from the target surface up to a distance of 2.4 mm, and then it falls down.

3.2.2 Axial profile of plasma temperature and density of LIP of Mo

The same atomic transitions are used to measure the plasma temperature at the various axial position of plasma as are listed in Table 1. The spatial variation in plasma temperature obtained from the Boltzmann plot Eq. (1) is shown in Fig. 9a.

It follows a similar trend as that of the intensity profile of MoI line, the temperature approaches a maximum value at a position of 2 mm distance from the target surface for the incident laser energy of 25 mJ and for other higher laser energies it is at 2.4 mm from the target surface. This is in agreement with that of the reported in the literature [4, 11, 14, 45–47]. The value of the temperature is increasing with incident laser energy. After the 4 mm distance from the target, it is not possible to estimate the plasma temperature correctly as the intensity is extremely low.



The electron density profile distribution along the plasma axis for various laser energies obtained from Eq. (3), is shown in Fig. 9b. From the Fig. 9b, it is evident that the electron density reaches a maximum value at a distance of 2 mm away from the target. Normally it is expected that the electron density decreases away from the target surface but in the present study spatial profile is recorded at a fixed delay of 2 μ s, at which the LIP is already detached and moving away from the targets and simultaneously expanding. The maxima of the electron density and temperature are always within its core. Thus, both these parameters attain the maximum value at a certain distance away with respect to the target at a later time scale.

3.2.3 Assessment of LTE along the axial direction of the plasma plume

The Fig. 10a displays the estimated minimum value of electron density as per Mc-Whirter criteria from Eq. (4) as a function distance from the target at all the four values of incident laser energies. Close to the target surface, the value of the estimated electron density is $1.47 \times 10^{16} \text{ cm}^{-3}$ while the required electron density from Mc-Whirter criteria is $4.58 \times 10^{16} \text{ cm}^{-3}$ for the incident laser energy of 25 mJ. So, the minimum value is less than one order of magnitude than that of the experimentally measured electron density thus confirming the LTE in the entire spatial region. The diffusion length is estimated by Eq. (10) as a function of distance and is shown in Fig. 10b. At all the locations within the LIP, the diffusion length is of the order 10^{-4} mm which much less than the overall dimension of the plasma further confirming the LTE condition in the case of inhomogeneous LIP.

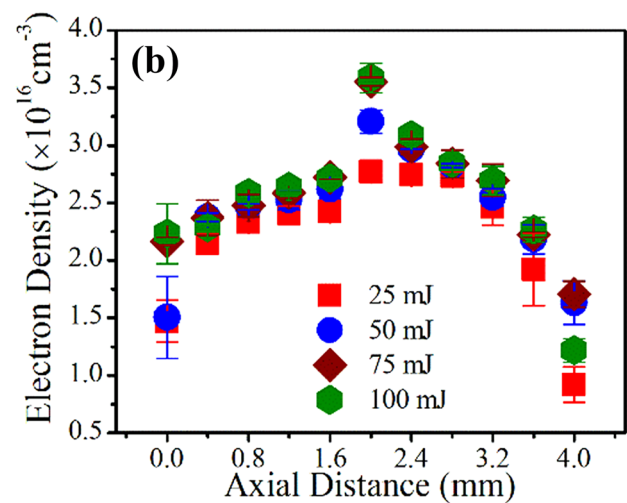


Fig. 9 a Temperature and b electron density variation along the axial direction of the plasma at different laser energies

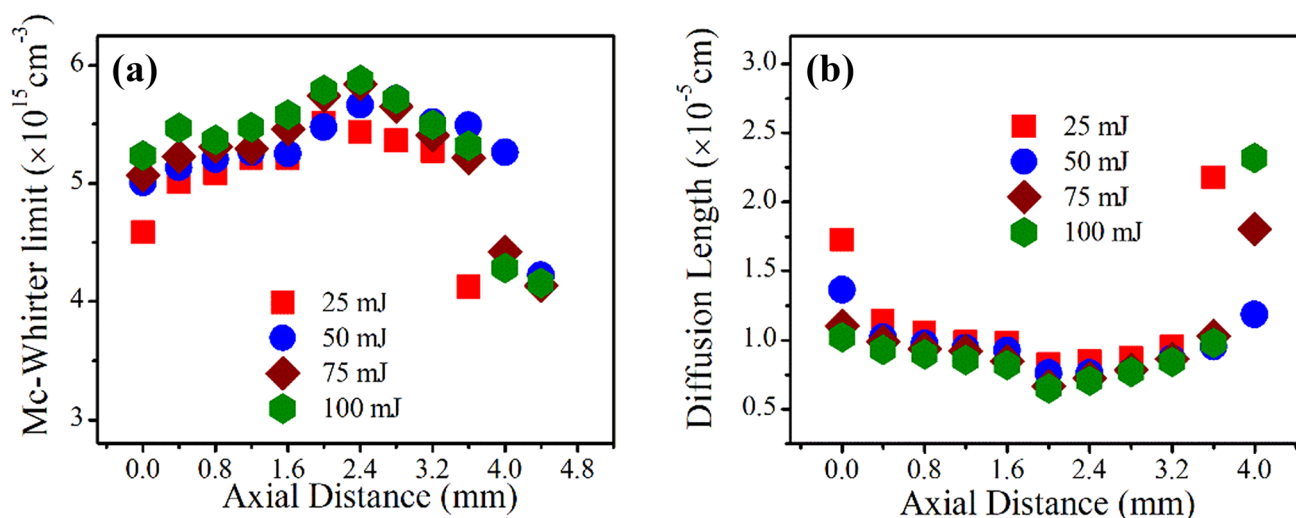


Fig. 10 **a** Minimum required electron density for LTE, **b** diffusion length of the plasma at the various axial position at various energies

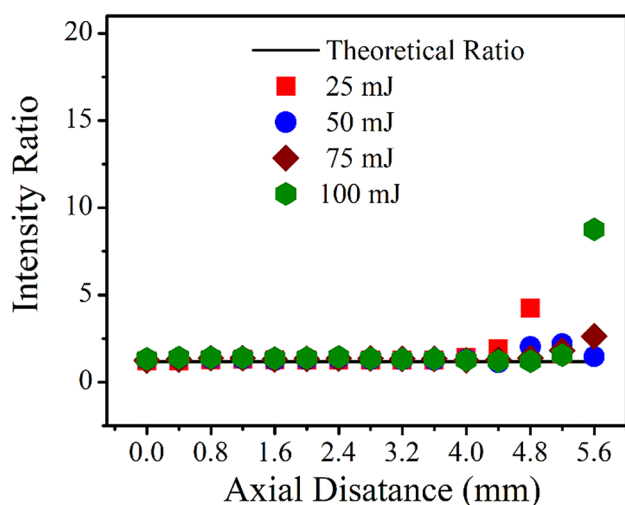


Fig. 11 Variation of the intensity ratio of MoI-568.9/579.1 at different location along the direction of expansion as a function of laser energy

3.2.4 Spatial window for the optically thin condition of LIP of Mo

In space-resolved studies, the same pair of MoI lines are used for branching ratio as mention in the Sect. 3.1.4 for the temporal evolution to investigate the optical thin condition of LIP in various segments of plasma and the experimental results are shown in Fig. 11. The experimental intensity and for MoI-568.9/MoI-579.1 nm, are in close proximity of the theoretically estimated values, Eq. (11), up to a distance of away 4 mm from the target at all the energies and it deviates beyond this distance from the target.

4 Conclusion

The purpose of the present work is to study the LIP of Mo in air using time and space-resolved LIBS as a function of incident laser energy to get the optimized temporal and spatial window where the LTE and optical thin conditions are valid. The LIP emission intensity of atomic and ionic lines, plasma temperature and electron density are studied in both cases. From the temporal evolution, it is observed that the emitted line intensity of LIP and the plasma parameters are decaying with the increase in delay time from 0.5 to 5 μs . All these parameters increase with an increase in the incident laser energies. The intensity of atomic lines persist for a longer time duration than that of the ionic lines and the decay time of atom and ion increases with the increase of incident laser energy. The SNR of the spectra initially increases up to delay time of 3.5 μs and beyond this it falls down. The plasma temperature estimated from MoI and MoII lines separately, acquires nearly the same value in the temporal window of 1.5–4 μs thus affirming the coexistence of thermal equilibrium among atoms and ions. The LTE condition is verified by Mc-Whirter criteria as well as considering the transient nature of plasma. The obtained relaxation time is of 10^{-10} s is much less than the plasma decay time, of the order of 10^{-6} s. Both these observations confirm the validity of LTE in the LIP. The LIP is observed to be optically thin in the temporal window of 1.5–5 μs as it is verified via branching ratio. So, from the temporal evolution of plasma emission intensity, SNR, plasma parameters as well as LTE and optically thin condition of plasma, an optimum temporal window for LIBS study is identified in the delay range of 1.5–3.5 μs with respect to laser pulse. The space-resolved spectra were recorded at different locations of the LIP plume along the axial plasma expansion direction. The maximum attainable value of the plasma emission intensity, the temperature and

electron density is found at a certain distance away from the target surface and decreases close to the target as well as towards the plasma edge. The maximum intensity for the ionic line appears slightly closer to the target as compared to that of the atomic lines. From the axial profile of plasma temperature, it is also observed that the maximum value is around at 2.4 mm from the target surface. The fall in temperature near to the target is less while a sharp fall towards the leading edge of the plasma is observed. From the axial profile of electron density, it is observed that it reaches a maximum value at a distance of 2 mm away from the target surface but decreases beyond this. The LTE criteria are verified in the case of inhomogeneous expansion of plasma. The experimentally obtained branching ratios are in good agreement with the theoretical ratios in the space-resolved studies up to the axial distance of 4 mm. Thus, the optimum spatial window is within the range of 0.8–3.2 mm from the target for all the laser energies. These studies on the LIP of Mo using time and space-resolved studies presented in the manuscript will be helpful in offering important reference data for the design and optimization of LIBS systems involved in various field of applications.

References

- G. Cristoforetti, G. Lorenzetti, S. Legnaioli, V. Palleschi, *Spectrochim. Acta, Part B* **65**(9–10), 787–796 (2010)
- J.D. Winefordner, I.B. Gornushkin, T. Correll, E. Gibb, B.W. Smith, N. Omenetto, *J. Anal. At. Spectrom.* **19**(9), 1061–1083 (2004)
- L.J. Radziemski, D.A. Cremers, *Laser-induced Plasmas and Applications* (Wiley, 2006)
- K.J. Grant, G.L. Paul, *Appl. Spectrosc.* **44**(8), 1349–1354 (1990)
- S. Harilal, P. Diwakar, N. LaHaye, M. Phillips, *Spectrochim. Acta, Part B* **111**, 1–7 (2015)
- M. Autin, A. Briand, P. Mauchien, J. Mermet, *Spectrochim. Acta, Part B* **48**(6–7), 851–862 (1993)
- M. Corsi, G. Cristoforetti, M. Giuffrida, M. Hidalgo, S. Legnaioli, V. Palleschi, A. Salvetti, E. Tognoni, C. Vallebona, *Spectrochim. Acta, Part B* **59**(5), 723–735 (2004)
- J. Freeman, S. Harilal, P. Diwakar, B. Verhoff, A. Hassanein, *Spectrochim. Acta, Part B* **87**, 43–50 (2013)
- C. Gautier, P. Fichet, D. Menut, J.-L. Lacour, D. L'Hermite, J. Dubessy, *Spectrochim. Acta, Part B* **59**(7), 975–986 (2004)
- X.L. Mao, M.A. Shannon, A.J. Fernandez, R.E. Russo, *Appl. Spectrosc.* **49**(7), 1054–1062 (1995)
- O. Barthélemy, J. Margot, M. Chaker, M. Sabsabi, F. Vidal, T. Johnston, S. Laville, B. Le Drogoff, *Spectrochim. Acta, Part B* **60**(7–8), 905–914 (2005)
- F. Colao, V. Lazic, R. Fantoni, S. Pershin, *Spectrochim. Acta, Part B* **57**(7), 1167–1179 (2002)
- S. Amoroso, *Appl. Phys. A* **69**(3), 323–332 (1999)
- Y.-I. Lee, S.P. Sawan, T.L. Thiem, Y.-Y. Teng, J. Sneddon, *Appl. Spectrosc.* **46**(3), 436–441 (1992)
- M. Gondal, Y. Maganda, M. Dastageer, F. Al-Adel, and A. Naqvi, Study of temporal evolution of electron density and temperature for atmospheric plasma generated from fluid samples using laser induced breakdown spectroscopy. In: *Electronics, Communications and Photonics Conference (SIECP), 2013 Saudi International* (IEEE, 2013), p. 1–4.
- F. Bredice, P.P. Martinez, C. Sánchez-Aké, M. Villagrán-Muniz, *Spectrochim. Acta, Part B* **107**, 25–31 (2015)
- S. Harilal, C. Bindhu, R.C. Issac, V. Nampoore, C. Vallabhan, *J. Appl. Phys.* **82**(5), 2140–2146 (1997)
- M.R. Joseph, N. Xu, V. Majidi, *Spectrochim. Acta, Part B* **49**(1), 89–103 (1994)
- B. Le Drogoff, J. Margot, F. Vidal, S. Laville, M. Chaker, M. Sabsabi, T. Johnston, O. Barthélemy, *Plasma Sources Sci. Technol.* **13**(2), 223 (2004)
- L.J. Radziemski, T.R. Loree, D.A. Cremers, N.M. Hoffman, *Anal. Chem.* **55**(8), 1246–1252 (1983)
- J. Aguilera, J. Bengoechea, C. Aragón, *Spectrochim. Acta, Part B* **59**(4), 461–469 (2004)
- L. Radziemski, T. Loree, *Plasma Chem. Plasma Process.* **1**(3), 281–293 (1981)
- T.N. Piehler, F.C. DeLucia, C.A. Munson, B.E. Homan, A.W. Miziolek, K.L. McNesby, *Appl. Opt.* **44**(18), 3654–3660 (2005)
- A. Mostako, A. Khare, *Laser Part. Beams* **30**(4), 559–567 (2012)
- M. Akram, S. Bashir, M.S. Rafique, A. Hayat, K. Mahmood, *Plasma Chem. Plasma Process.* **37**(1), 287–304 (2017)
- M. Wisse, L. Marot, A. Widdowson, M. Rubel, D. Ivanova, P. Petersson, R. Doerner, M. Baldwin, J. Likonen, E. Alves, *Fusion Eng. Des.* **89**(2), 122–130 (2014)
- Q.H. Wang, K. Kalantar-Zadeh, A. Kis, J.N. Coleman, M.S. Strano, *Nat. Nanotechnol.* **7**(11), 699 (2012)
- E. Mal, R. Junjuri, M.K. Gundawar, A. Khare, *J. Anal. At. Spectrom.* **34**, 319 (2019)
- NIST Atomic Spectra Database. https://physics.nist.gov/PhysRefData/ASD/lines_form.html
- Kurucz Database. <https://www.cfa.harvard.edu/amp/ampdata/kurucz23/sekur.html>
- P.J. Skrodzki, J.R. Becker, P.K. Diwakar, S.S. Harilal, A. Hassanein, *Appl. Spectrosc.* **70**(3), 467–473 (2016)
- J. Freeman, P. Diwakar, S. Harilal, A. Hassanein, *Spectrochim. Acta, Part B* **102**, 36–41 (2014)
- S. Zhang, X. Wang, M. He, Y. Jiang, B. Zhang, W. Hang, B. Huang, *Spectrochim. Acta, Part B* **97**, 13–33 (2014)
- C. Aragón, J.A. Aguilera, *Spectrochim. Acta, Part B* **63**(9), 893–916 (2008)
- J.B. Simeonsson, A.W. Miziolek, *Appl. Opt.* **32**(6), 939–947 (1993)
- J.A. Aguilera, C. Aragón, *Spectrochim. Acta, Part B* **59**(12), 1861–1876 (2004)
- E. Sternberg, N. Rodrigues, J. Amorim, *Appl. Phys. B* **122**(1), 21 (2016)
- A. Elhassan, A. Giakoumaki, D. Anglos, G. Ingo, L. Robbiola, M. Harith, *Spectrochim. Acta, Part B* **63**(4), 504–511 (2008)
- M. Akram, S. Bashir, M.S. Rafique, A. Hayat, K. Mahmood, A. Dawood, M. Bashir, *Appl. Phys. A* **119**(3), 859–870 (2015)
- G. Cristoforetti, A. De Giacomo, M. Dell'Aglio, S. Legnaioli, E. Tognoni, V. Palleschi, N. Omenetto, *Spectrochim. Acta, Part B* **65**(1), 86–95 (2010)
- T. Fujimoto, R. McWhirter, *Phys. Rev. A* **42**(11), 6588 (1990)
- J.P. Singh, S.N. Thakur, *Laser-Induced Breakdown Spectroscopy* (Elsevier, 2007).
- H. Hegazy, H.A. El-Ghany, S. Allam, T.M. El-Sherbini, *Appl. Phys. B* **110**(4), 509–518 (2013)
- Q. Ma, V. Motto-Ros, W. Lei, M. Boueri, X. Bai, L. Zheng, H. Zeng, J. Yu, *Spectrochim. Acta, Part B* **65**(11), 896–907 (2010)
- M. Hafez, M. Khedr, F. Elaksher, Y. Gamal, *Plasma Sources Sci. Technol.* **12**(2), 185 (2003)
- W. Luo, X. Zhao, Q. Sun, C. Gao, J. Tang, H. Wang, W. Zhao, *Pramana* **74**(6), 945–959 (2010)
- G. Abdellatif, H. Imam, *Spectrochim. Acta, Part B* **57**(7), 1155–1165 (2002)

Publisher's Note Springer Nature remains neutral with regard to jurisdictional claims in published maps and institutional affiliations.